# Carbon-modified $MgH_2$: Experimental and *ab-initio* Investigations

Toufic Tayeh[a,b,c], Abdel Salam Awad[a,b,c], Michel Nakhl[c], Jean-Louis Bobet[a,b], Mirvat Zakhour[c], and Samir F. Matar[a,b]

[a] Institut de Chimie de la Matière Condensée de Bordeaux-CNRS, UPR 9048, F-33600 Pessac, France

[b] Université Bordeaux 1, Institut de Chimie de Université de Bordeaux, UPR 9048, F33600 Pessac, France

[c] Lebanese University, LCPM, Fanar, Beirut, Lebanon

Reprint requests to Samir F. Matar. E-mail: matar@icmcb-bordeaux.cnrs.fr

*Z. Naturforsch.* **2014**, *69b*, 804 – 810 / DOI: 10.5560/ZNB.2014-4072
Received March 19, 2014

The results of experimental and theoretical investigations of carbon-modified $MgH_2$ for improving its sorption performances in hydrogen storage devices are reported. Large changes on its absorption/desorption capacities have been found. The following aspects are considered: size effects where finer particles obtained by energetic ball milling enable easier penetration, catalytic effects of carbon at the surface, and entrance of small quantities of C interstitially into the $MgH_2$ structure. The energies and charge densities as studied by DFT suggest the activation of $MgH_2$ through a decrease of the cohesive energy of the pristine hydride and a reduced ionic charge on hydrogen.

*Key words:* Magnesium Hydride, Ball Milling, Carbon Doping, DFT, ELF

## Introduction

Hydrogen is one of the most attractive energy carriers because of its high energy density and low carbon emission [1 – 4]. In order to maximize its use, safe and efficient ways to store and deliver hydrogen need to be developed. Magnesium is a potential candidate for hydrogen storage due to its abundance, low cost and non-toxic nature. Its high theoretical gravimetric capacity of 7.6 wt.-%, low density and reversibility make it an attractive material for hydrogen storage [5 – 7]. However, despite these advantages, the hydrogen absorption/desorption at standard conditions need to be improved. The high binding energy between magnesium and hydrogen (74.7 kJ $mol^{-1}$ of $H_2$) requires high temperature above 300 °C to release hydrogen [8]. This makes difficult the direct use of $MgH_2$ in storage devices. Many studies over the last years have concentrated on efforts to improve the absorption/desorption kinetics of $MgH_2$ by *p*-type elements such as carbon [9 – 11] or transition metals such as Ni, Fe, Ti, and V [12, 13]. The transition metal catalysts are known to promote the dissociation/recombination of hydrogen thereby resulting in fast hydrogen absorption/desorption. Introducing nickel leads to materials with reversible hydrogen absorption ability such as in $Mg_2NiH_4$ [14, 15]. The formation of $MgH_2$/carbon nanotube composites by ball milling was shown to improve hydrogen absorption/desorption kinetics [16]. Recently, we have shown that magnesium mixed with graphite by ball milling enhances the absorption properties [17]. No experimental work has been reported on a possible presence of carbon within the structure. The insertion of carbon or other light elements of the first period into $MgH_2$ should not change much the gravimetric density necessary for applications, while modifying the electronic structure such as the cohesive energy and the charge on hydrogen, and therefore the absorption/desorption capacity. We have shown that the ionic character of hydrogen in ionic hydrides is strongly reduced by selective substitutions of Mg by Ni [18].

This manuscript is divided into two parts; a first experimental part relates to the formation by mechanical grinding of Mg/carbon fiber materials and the measurements of the hydrogen sorption kinetics. A second part presents a theoretical approach investigating the

effects of the presence of foreign elements such as carbon entering the $MgH_2$ structure interstitially as based on computations within the well established quantum-theoretical density functional DFT framework [19, 20].

## Experimental Section

Mg (Strem Chemicals, 99.9 %) and carbon fibers (R-A301; TEIJIN LIMITED) were used as starting materials. Ball milling was performed during 10 h under 10 bars of hydrogen using stainless-steel jar and balls, with a ball-to-powder mass ratio of 19 : 1 using a planetary ball miller type Fritsch pulverisette 5 to produce (i) a nanostructured magnesium and (ii) two composite materials Mg/5 wt.-% carbon fibers and Mg/10 wt.-% carbon fibers. The samples were characterized by X-ray diffraction (XRD) using a Philips PANalytical X'Pert (PW1820) diffractometer with Cu$K_{\alpha 1}$ radiation. The crystallite sizes were determined from the peak broadening using the Williamson-Hall plot. Particle size and morphology were studied by scanning electron microscopy (SEM) using a Tescan VEGA3 SB microscope. The C2-3000 automatic cycler of Hera Hydrogen Systems® was used for the measurement of the hydrogen sorption kinetics of the materials.

## Results and Discussion

The X-ray diffractograms of commercial Mg and of the Mg/10 wt.-% carbon fiber samples ball milled for 1, 3, 5, and 10 h are shown in Fig. 1. With increasing the milling time, the intensity of the Mg characteristic peaks decreases (*i. e.* decrease in crystallite size and/or transformation of the phase). The appearance of characteristic peaks of magnesium hydride after 3 h of grinding means that the transformation of magnesium into its hydride begins. In addition, the disappearance of the characteristic peak of carbon at 26° indicates that the fibers were broken during the grinding (*i. e.* decrease of their crystalline character) and dispersed in the Mg matrix. Finally, an interesting change in the relative intensity of the peaks of Mg (101) and Mg (002) was observed after 1 h of milling, indicating that preferential orientation is induced along the crystallographic *c* axis. This result is similar to the one obtained in Grosjean and Yongan's works [21, 22]. The energy required to achieve this deformation by sliding perpendicular to the *c* axis is significantly lower than in other directions. Thus, deformations are much easier to generate. However, the accumulation of energy

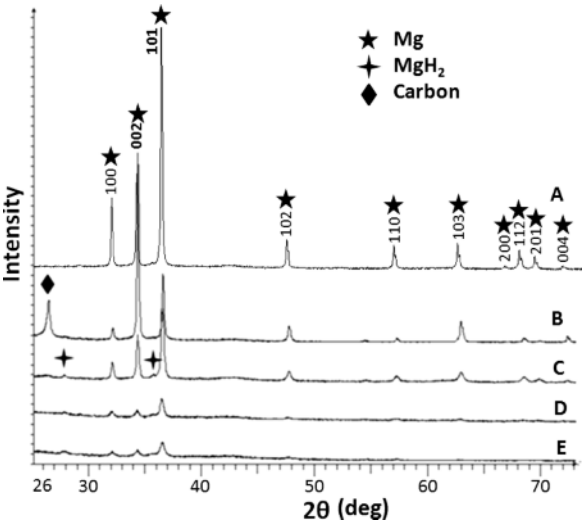


Fig. 1. X-Ray diffractograms of commercial Mg powder (A), ball-milled with 10 wt.-% carbon fibers (Cf) for 1 h (B), 3 h (C), 5 h (D) and 10 h (E).

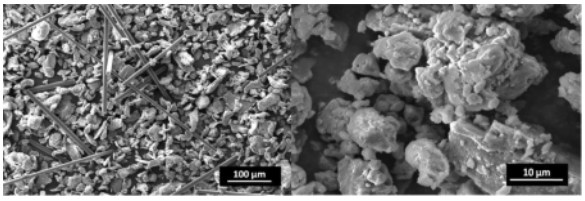


Fig. 2. SEM micrographs showing the Mg + Cf mixture before grinding (left) and after grinding (right).

after prolonged grinding (from > 3 h) leads to a random deformation of the powder and a loss of the (002) texture.

Fig. 2 presents two micrographs: The first (left) shows sticks of carbon fibers (Cf), between the particles of magnesium, and the second (right) shows an intimate mixture of the two components after mechanical grinding. These two micrographs also show the reduction in the particles size after grinding. We note that this size has changed from a few tens of microns before ball milling to only a few microns after treatment of the agglomerates.

The absorption kinetics at 300 °C under 10 bars of $H_2$ and the desorption at 330 °C under 0.3 bar of commercial Mg and of samples ball-milled for 10 h without additives or with 5 % and 10 % by weight of Cf are shown in Figs. 3 and 4. The addition of carbon fibers improves the hydrogen sorption kinetics but also decreases the maximum storage capacity of magnesium

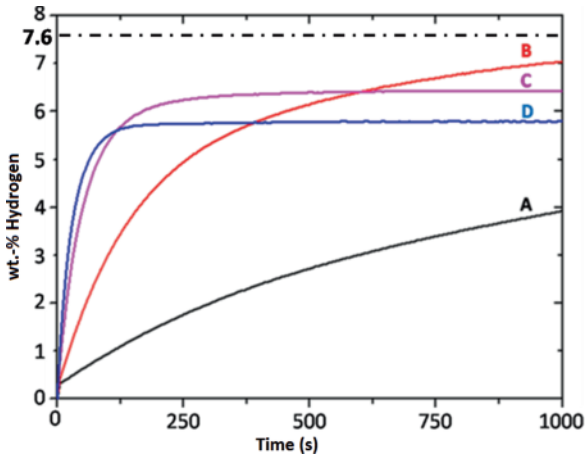


Fig. 3 (color online). Absorption kinetics at 300 °C for commercial Mg (A), for the 10 h ball-milled sample without any additions (B), with 5 wt.-% Cf (C) and with 10 wt.-% Cf (D).

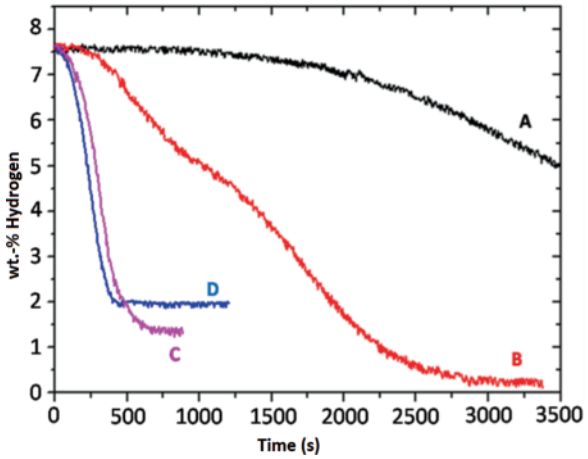


Fig. 4 (color online). Desorption kinetics at 330 °C for commercial Mg (A), for the 10 h ball-milled sample without any additions (B), with 5 wt.-% Cf (C) and with 10 wt.-% Cf (D).

(*e. g.* proportionally to the amount of added carbon). These results are similar to those found in the literature [23 – 28].

In view of the results, three assumptions can be made: (i) carbon fibers help obtaining finer particles during grinding, creating new paths for the penetration of hydrogen as well as a larger contact surface powder/gas, (ii) carbon acts as a catalyst on the surface of the particles, which helps in the decomposition of $H_2$ molecules, and (iii) small amounts of carbon atoms can enter the $MgH_2$ structure as interstitials affecting the strength of the Mg–H chemical bond. This assumption is analyzed below.

## Computational Section

For the quantum mechanical DFT modeling of carbon presence within $MgH_2$ the Vienna *ab-initio* simulation package (VASP) [29, 30] was used. This package allows geometry optimization and total energy calculations. For this we use the projector augmented wave (PAW) method [30, 31], built within the generalized gradient approximation (GGA) scheme following Perdew, Burke and Ernzerhof (PBE) [32] and accounting for the valence electrons. Including semi-core Mg $2p^6$ states in the PAW potentials is necessary to avoid a too large ionic character of H as $H^{-1}$ which would be obtained by a full departure of two electrons from Mg. Preliminary calculations with local density approximation LDA [33] led to an underestimated volume *versus* the experiment: $V_{LDA}(MgH_2) = 55.6$ Å$^3$ and $V_{GGA}(MgH_2) = 58.2$ Å$^3$. The tetrahedron method with Blöchl corrections [31] as well as a Methfessel-Paxton [34] scheme were applied for both geometry relaxation and total energy calculations. Brillouin zone (BZ) integrals were approximated using the special *k*-point sampling [34]. The optimization of the structural parameters was performed until the forces on the atoms were less than 0.02 eV Å$^{-1}$ and all stress components less than 0.003 eV Å$^{-3}$. The calculations converged at an energy cut-off of 400 eV for the plane-wave basis set with respect to the k-point integration with a starting mesh of $4 \times 4 \times 4$ up to $8 \times 8 \times 8$ for best convergence and relaxation to zero strain. From the calculations, an illustration of the electron distribution is available from the electron localization function (ELF) [35, 36]. ELF is a normalized function between 0 (zero localization, blue zones) and 1 (strong localization, red zones) with the value of $^1/_2$ corresponding to a free electron gas behavior (green zones), *cf.* Fig. 5. An analysis of the charge density is done with the Atoms in Molecules and Crystals approach (AIM) introduced by Bader [37] who developed an intuitive way of dividing molecules into atoms as based purely on the electronic charge density. For each atom in the compound, Bader considers it as surrounded by a surface running through minima of the charge density. Then the total charge of an atom is determined by integration within the Bader region. Such an analysis can be useful when trends of charge transfer are sought; they do not constitute a tool

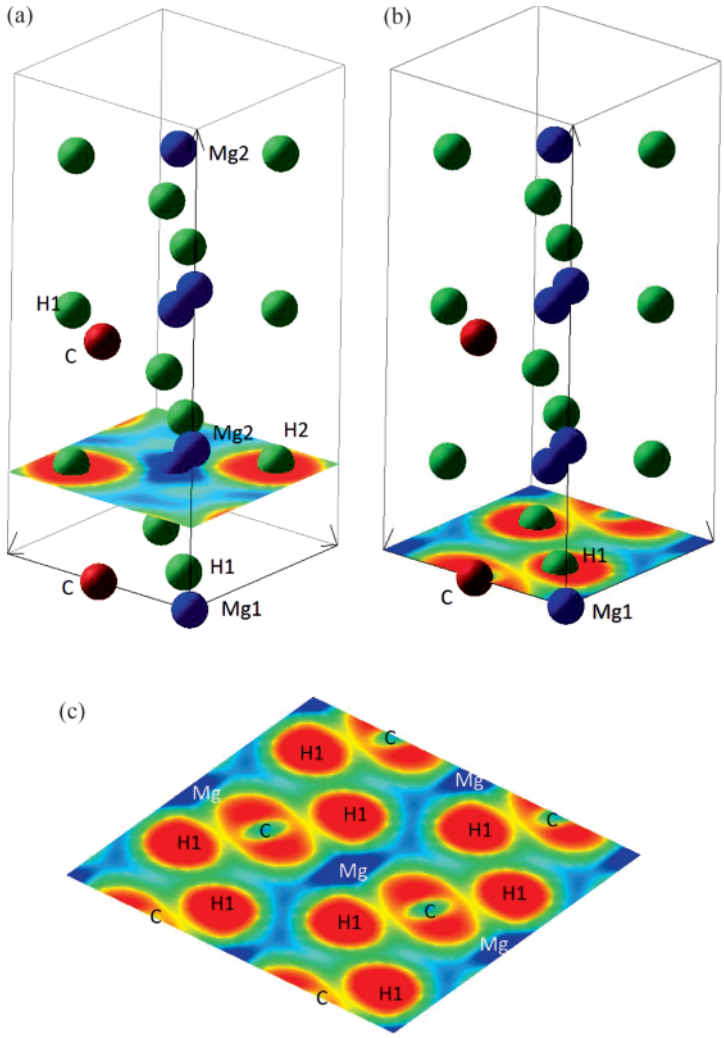


Fig. 5 (color online). Trirutile model structure for $MgH_2$ with electron localization function (ELF) slices perpendicular to the crystallographic *c* axis showing planes at a) Mg2, H2 and b) at Mg1, H1 with carbon; c) extended ELF slice over 4 cells comprising Mg2, H1 and C.

for evaluating absolute ionizations. In the presently studied compounds we evaluate the changes in total charge on H in $MgH_2$ and the carbon-modified compound.

*Building of a model crystal structure*

The rutile structure $AX_2$ does not allow the observation of local modifications because of the presence of only one equivalent of A. One solution is to find a candidate model based on rutile. From the extensive discussion of rutile-type derivatives by Baur [38], orthorhombic $CoReO_4$, $MgUO_4$ types and trirutile could be envisaged. However, the latter appears to be the best choice because it has the same tetragonal symmetry as simple rutile with space group $P4_2/mnm$ and six formula units (FU) per cell (Table 1 and Fig. 5). Also the insertion of a foreign element can be done selectively to chemically affect one of the six Mg atoms in the trirutile cell, namely the Mg1 site (two equivalents: one at the origin and one at $^1/_2$, $^1/_2$, $^1/_2$) and its neighboring H1 whereas Mg2 (four equivalents) and its neighbor-

Table 1. Geometry-optimized lattice parameters and energies for $MgH_2$ in the trirutile $Mg_3H_6$ structure and C-inserted $Mg_3H_6$. C is at (4*c*: 0, ½, 0; ½, 0, ½; ½, 0, 0; 0, ½, ½). Experimental $E_{coh} = -0.79$ eV per mole of $H_2$ [40].

| Hydride | $Mg_3H_6$ | C:$Mg_3H_6$ |
|---|---|---|
| *a* (Å) | 4.246 | 4.228 |
| *c*/*a* | 2.232 | 2.615 |
| | | |
| Mg1 (0, 0, 0) | 0 | 0 |
| Mg2 (0, 0, *z*) | 0.303 | 0.326 |
| H1 (*x*, *x*, 0) | 0.303 | 0.298 |
| H2 (*y*, *y*, *z*′) | 0.304, 0.334 | 0.314, 0.318 |
| | | |
| *V* (Å$^3$) | 170.86 | 195.88 |
| Energy (eV) | −54.82 | −69.70 |
| $E_{coh}$ per $H_2$ (eV) | −0.81 | −0.13 |

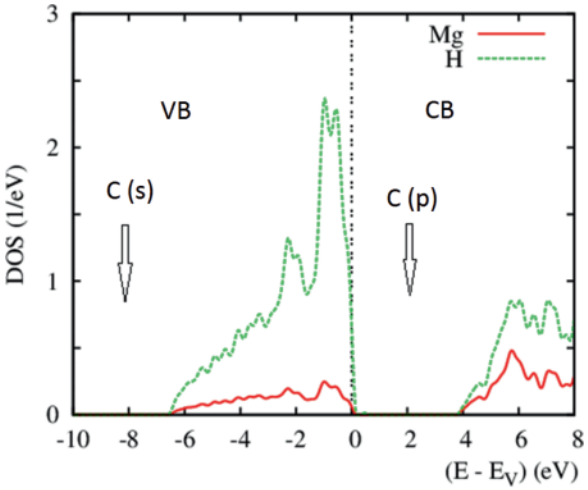


Fig. 6 (color online). Electron density of states of $MgH_2$ representing the carbon *s* and *p* states entering respectively at the bottom and the top of the valence band.

ing H2 should be less subjected to direct effects of the *p* element as depicted in Fig. 5.

It needs to be noted that the rutile structure presents several interstitial sites. The diffusion of foreign chemical species such as lithium into rutile $TiO_2$ was studied by Kingsbury *et al.* [39] using semi-empirical Born-Mayer potentials. The authors considered the (8*i*), the (4*c*) and (4*d*) positions with the latter two as energetically most favored and with little energy difference between them. We here consider the insertion effects of carbon.

*Geometry optimization and cohesive energies*

The results of the calculation for trirutile $Mg_3H_6$ are given in Table 1. The volume $V = 175.1$ Å$^3$ *i. e.* 58.4 Å$^3$ per FU, is 5% smaller than the experimental value of 61.6 Å$^3$. Regarding the total energy, it is important to check the cohesive energy per $H_2$ pair with respect to the experiment. Following the experimental work of Yamaguchi *et al.* [40], the cohesive energy of $MgH_2$ per mole of dihydrogen ($H_2$) is $E_{coh} = -0.79$ eV. For the purpose of approaching the experiment, the energies of the constituents were calculated: Mg (hexagonal, with $2p^6$ semi-core states) $= -2.784$ eV (2 FU); dihydrogen (in a large box) $= -6.93$ eV; C (hexagonal) $= -9.49$ eV (2 FU). The cohesive energy per H–H pair is then obtained: $E_{coh}(Mg_3H_6) = -0.81$ eV in good agreement with the experiment [40]. This provides reliability for the computational method and the trirutile model structure.

The calculations for the insertion of carbon at 0, ½, 0 (Wyckoff position 4*c*), *i. e.* with four equivalents, provide the results given in the 2$^{nd}$ column of Table 1. Changes of the atomic positions and of the volume are observed especially for the large volume increase expected from the added extra atoms. Also the internal coordinates are slightly modified. The relevant feature is the strong reduction of the cohesive energy down to –0.13 eV per $H_2$. The large amount of inserted C in the model host strongly destabilizes the hydride so that less carbon content could be tolerated interstitially. Further calculations with one carbon atom out of the four led to a cohesive energy $E_{coh} = -0.44$ eV per $H_2$ which is then close to half the magnitude of $E_{coh}(MgH_2)$. It may be concluded that small amounts of inserted carbon are likely to induce large effects on the electronic structure, and the energy destabilization of $MgH_2$ with carbon is in favor of the aimed $MgH_2$ activation for potential use in devices.

*Changes of the ionic-covalent character and of the electronic structure*

The results can be further assessed using a charge analysis within Bader's Theory of Atoms in Molecules (AIM) introduced above [37]. For the pristine hydride the large ionic character of $MgH_2$ has been confirmed by the calculations with an average charge of $H^{-0.82}$ also obtained by others [41].

Upon the insertion of one carbon in the neighborhood of Mg1, at either one of the planes shown in

Fig. 5, there is a lowering of the ionic character of H1 down to −0.25, and to −0.71 for H2 which is in the neighborhood of Mg2. The role of carbon which becomes negatively charged is to drain electrons from hydrogen. This is obvious from the large change in the hydrogen ionic character in the neighborhood of carbon but also at the other hydrogen sites. This is illustrated in Fig. 5 showing the ELF slices at horizontal planes crossing Mg2, H2 (Fig. 5a) and Mg1, H1 with carbon (Fig. 5b) for a calculation accounting for a reduced number of carbon atoms, two out of four at position 4*c*. An ionic-like behavior close to that of $MgH_2$ is observed in Fig. 5a from the strong localization (red contours with ELF ∼ 0.8) around H2 while no localization (blue contours with ELF ∼ 0.1) characterizes Mg2. On the opposite, the ELF slice showing the Mg1, H1 plane (Fig. 5b) exhibits a different character with electron localization around H1 extending to carbon. This is further elaborated in Fig. 5c showing an extended ELF slice over 4 adjacent cells. In panels b) and c) the blue areas of zero localization are reduced to the immediate neighborhood of Mg1 in comparison to panel a).

These observations are indicative of an overall change of the electronic structure due to the carbon insertion. $MgH_2$ is an insulator with a large band gap of ∼ 4 eV at the top of the valence band $E_V$ as shown in Fig. 6. The valence band (VB) and the conduction band (CB) are dominant with H partial DOS (PDOS) whereas the Mg PDOS show lower magnitude. This is not only due to the twice larger number of H in the structure but also to the transfer of electrons from Mg to H leading to a more hydridic (ionic) character. Carbon PDOS have been shown by the calculation to be schematically at the bottom of the VB for carbon *s* states and shifted into the gap for carbon *p* states.

## Conclusion

Carbon-modified samples of the ionic hydride $MgH_2$ have been shown experimentally to have improved absorption/desorption capacities for hydrogen. A proposition is made and confirmed by *ab initio* investigations that small amounts of carbon inserted into the crystal structure are likely to drastically change the ionic-covalent character of hydrogen through draining of electrons. Small quantities of carbon introduced into Mg melts are being tested [42] to bring further support for the theoretical findings regarding the chemical effects in composites C:$MgH_2$ or the local formation of magnesium carbides.


[1] C.-J. Winter, *Int. J. Hydrogen Energy* **2009**, *34*, S1.
[2] S. M. Khantimerov, N. M. Suleimanov, E. F. Kukovitsky, O. I. Gnezdilov, V. L. Matukhin, Yu. A. Sakhratov, *Int. J. Hydrogen Energy* **2011**, *36*, 1216.
[3] M. Ball, M. Wietschel, *Int. J. Hydrogen Energy* **2009**, *34*, 615.
[4] M. Balat, *Int. J. Hydrogen Energy* **2008**, *33*, 4013.
[5] K. Zeng, T. Klassen, W. Oelerich, R. Bormann, *Int. J. Hydrogen Energy* **1999**, *24*, 989.
[6] B. Sakintuna, F. Lamari-Darkrim, M. Hirscher, *Int. J. Hydrogen Energy* **2007**, *32*, 1121.
[7] L. Schlapbach, A. Zuttel, *Nature* **2001**, *414*, 353.
[8] K. F. Aguey-Zinsou, J. R. Ares-Fernandez, *Energy Environ. Sci.* **2010**, *3*, 526.
[9] H. Imamura, Y. Takesue, T. Akimoto, S. Tabata, *J. Alloys Compd.* **1999**, *293*, 564.
[10] F. J. Castro, V. Fuster, G. Urretavizcaya, *J. Alloys Compd.* **2011**, *509*, 595.
[11] J.-L. Bobet, E. Grigorova, M. Khrussanova, M. Khristov, P. Stefanov, P. Peshev, D. Radev, *J. Alloys Compd.* **2004**, *366*, 298 – 302.
[12] G. Liang, J. Huot, S. Boily, N A Van, R. Schulz, *J. Alloys Compd.* **1999**, *292*, 247.
[13] A. Zaluska, L. Zaluski, J. O. Strom-Olsen, *J. Alloys Compd.* **1999**, *288*, 217.
[14] J. J. Reilly, R. H. Wiswall, Jr., *Inorg. Chem.* **1968**, *7*, 2254.
[15] W. R. Myers, L.-W. Wang, T. J. Richardson, M. D. Rubin, *J. Appl. Phys.* **2002**, *91*, 15.
[16] C. Z. Wu, P. Wang, X. Yao, C. Liu, D. M. Chen, G. Q. Lu, H. M. Cheng, *J. Alloys Compd.* **2006**, *420*, 278.
[17] M. Nakhl, M. Zakhour, Ch. Amine, H. El-Rassy, S. F. Matar, *Adv. Mater. Res.* **2011**, *324*, 119.
[18] A. F. Al Alam, S. F. Matar, N. Ouaini, *Chem. Phys. Lett.* **2011**, *516*, 174.
[19] P. Hohenberg, W. Kohn, *Phys. Rev.* **1964**, *136*, B 864.
[20] W. Kohn, L. J. Sham, *Phys. Rev.* **1965**, *140*, A 1133.
[21] M. H. Grosjean, M. Zidoune, L. Roue, J. Huot, R. Schulz, *Electrochim. Acta* **2004**, *49*, 2461.
[22] L. Yongan, W. Xinhua, D. Zhaohui, L. Haizhen, L. Shouquan, G. Hongwei, Y. Mi, *Energy* **2013**, *53*, 147.

[23] A. Chaise, P. de Rango, Ph. Marty, D. Fruchart, S. Miraglia, R. Olives, S. Garrier, *Int. J. Hydrogen Energ.* **2009**, *34*, 8589.
[24] M. A. Lillo-Rodenas, Z. X. Guo, K. F. Aguey-Zinsou, D. Cazorla-Amoros, A. Linares-Solano, *Carbon* **2008**, *46*, 126.
[25] H. Imamura, N. Sakasai, T. Fujinaga, *J. Alloys Compd.* **1997**, *253*, 34.
[26] J. Huot, M. L. Tremblay, R. Schulz, *J. Alloys Compd.* **2003**, *356*, 603.
[27] Z. G. Huang, Z. P. Guo, A. Calka, D. Wexler, J. Wu, P. H. L. Notten, *Mater. Sci. Eng. A* **2007**, *447*, 180.
[28] J.-L. Bobet, E. Grigorova, M. Khrussanova, M. Khristov, P. Stefanov, P. Peshev, D. Radev, *J. Alloys Compd.* **2004**, *366*, 298.
[29] G. Kresse, J. Furthmüller, *Phys. Rev. B* **1996**, *54*, 11169.
[30] G. Kresse, J. Joubert, *Phys. Rev. B* **1999**, *59*, 1758.
[31] P. E. Blöchl, *Phys. Rev. B* **1994**, *50*, 17953.
[32] J. Perdew, K. Burke, M. Ernzerhof, *Phys. Rev. Lett.* **1996**, *77*, 3865.
[33] D. M. Ceperley, B. J. Alder, *Phys. Rev. Lett.* **1980**, *45*, 566.
[34] H. J. Monkhorst, J. D. Pack, *Phys. Rev. B* **1976**, *13*, 5188.
[35] A. D. Becke, K. E. Edgecombe, *J. Chem. Phys.* **1990**, *92*, 5397.
[36] A. D. Becke, K. E. Edgecombe, *Nature* **1994**, *371*, 683.
[37] R. Bader, *Chem. Rev.* **1991**, *91*, 893.
[38] W. H. Baur, *Z. Krist.* **1994**, *209*, 143.
[39] P. I. Kingsbury, Jr., W. D. Ohlsen, O. W. Johnson, *Phys. Rev.* **1968**, *175*, 1099.
[40] M. Yamaguchi, E. Akiba in *Materials Science and Technology*, Vol. 3B (Eds.: R. W. Cahn, P. Haasen, E. J. Kramer), VCH, New York **1994**, pp. 333.
[41] P. Vajeeston, P. Ravindran, H. Fjellvåg, *Nanotechnology* **2008**, *19*, 275704.
[42] J. Huot, Université du Quebec à Trois-Rivières, Trois-Rivières, Canada, unpublished results and private communication, **2013**.